Smoothing of deuterium-tritium ice by electrical heating of the saturated vapor

E. R. Mapoles,[1] J. Sater,[2] J. Pipes,[3] and E. Monsler[3]
[1]*Lawrence Livermore National Laboratory, P.O. Box 5508, L-481, Livermore, California 94550*
[2]*W. J. Schafer Associates, Inc., 303 Lindbergh Avenue, Livermore, California 94550*
[3]*Allied Signal Incorporated, 2021 Las Positas Court, Livermore, California 94550*
(Received 30 September 1996)

High gain targets for inertial confinement fusion (ICF) are spherical shells which contain a layer of deuterium-tritium (DT) ice which surrounds a volume of DT gas in thermal equilibrium with the solid. The roughness of the inner surface of the cryogenic fuel layer inside of these targets is one of the sources of imperfections which cause implosions to deviate from perfect one-dimensional performance. Reductions in the surface roughness of this fuel layer improve confidence in the ability of the ICF program to achieve ignition in the National Ignition Facility (NIF), and increase the relevance of cryogenic experiments on the omega laser. We have developed a technique to generate a heat flux across this surface by applying an electric field to the DT vapor in the center of these shells. This vapor has a small but significant conductivity due to ionization caused by β decay of tritium in the vapor and the solid. We describe here experiments using a 1.15 GHz cavity to apply an electric field to frozen DT inside of a sapphire test cell. The cell and cavity geometry allows visual observation of the frozen layers. We find that the resulting heat flux reduces the roughness of the ice surface. [S1063-651X(97)13803-X]

PACS number(s): 51.50.+v, 28.52.Cx, 78.70.Gq, 64.70.Hz

I. INTRODUCTION

All high gain target designs for inertial confinement fusion (ICF) employ uniform layers of condensed deuterium-tritium (DT) to achieve efficient ignition of the fuel [1]. Various routes to the formation of these layers within target shells have been investigated [2], and the most promising method relies on the radioactive self-heating of condensed DT to redistribute the solid along the isotherms in the structure containing the fuel [3–5]. This process is referred to as ''β layering.'' The resulting roughness of the ice surface has been characterized optically and been found to be in the range of 1–1.5 μm rms for cylindrical layers approximately 100 μm thick and 2 mm in diameter. It is desirable to reduce this roughness to reduce the effects of mix during the implosion of an ICF capsule and increase the drive flexibility available to experimental designers [6].

When liquid DT freezes in an isothermal shell, it initially forms a very rough layer on the bottom of the container. Because the ice heats itself with a volumetric rate of $q_s = 5.06 \times 10^{-2}$ W/cm^3, there are variations in the temperature of the surface of the ice as the film thickness varies. The thicker areas of the film are warmer and consequently have higher vapor pressures, so material tends to sublime away from these regions and recondense at the cooler areas. If the container is isothermal, this leads to an ice surface that conforms to the surface of the container. For pure DT the rate at which the material migrates can be shown to be [5] $R_{\mathrm{DT}} = q_s / s\rho_s$, where s is the heat of sublimation (1550 J/mol), and ρ_s (5.18×10^{-2} mol/cm^3) is the density of the solid, so that $1/R_{\mathrm{DT}} \approx 27$ min.

Once the ice layer has formed, the temperature within the ice layer is $T(x) = -q_s x^2/2k_s + q_s h x/k_s + T_0$, where k_s is the thermal conductivity of the solid, x is the distance from the inner edge of the container, h is the thickness of the ice, and T_0 is the temperature of the container. For wavelengths that are large compared to the surface thickness, the derivative of the temperature of the ice surface with respect to the ice thickness becomes $dT(h)/dh = q_s h/k_s$ at the free surface of the ice. For 100 μm of DT ice this is 0.15 K/cm. Since the increase in surface temperature with increasing surface thickness is driving the smoothing process, we expect that an increase in $dT(h)/dh$ should result in a smoother surface. One way to increase this quantity is to add an additional heat flux from the saturated vapor to the ice. A heat flux f_s, will generate an additional temperature profile in the ice, $T(x) = f_s x/k_s$, and will increase $dT(h)/dh$ by f_s/k_s. This increase will match the derivative produced by the DT self-heating when $f_s = q_s h$ or 5×10^{-4} W/cm^2.

Here we describe a method to generate a heat flux inside of an ICF target using the electrical conductivity of the DT vapor inside of the ice shell. This gas is made electrically conducting by the β decay of tritons in the gas and the surrounding fuel layer. An applied electric field heats this gas, generating a heat flux which propagates through the ice layer to the exterior of the shell.

II. ELECTRICAL CONDUCTIVITY OF DT

The electrical properties of DT gas are only roughly known but measurements have been made by Souers [7,8], using an ac bridge at low frequencies and low electric fields. These data may be used to estimate the free electron density in DT gas with a density of 100 mol/m^3 to be 4×10^{13} m^3 at 20 K. However, these measurements were done on the gas alone without the additional radiation load of the surrounding DT solid found in an ICF target. Souers [9] estimates the fraction of β particle energy escaping from a surface layer of DT of density 1.4 mol/m^2 as 0.11. This is about five times the β energy generated in the vapor of an ICF target. Since the free electrons are only about one percent of the charged particles in the gas [7,8], their recombination rate is approxi-

mately independent of density and we can estimate the free electron density in the gas as 2×10^{14} m^3. The electron mobility μ_e can be estimated from electron mobilities measured in 76.8 K D_2 gas [10] and from Ref. [9]. For fields of 500 V/cm and densities of 100 mol/m^3 these give $\mu_e=0.1$ m^2/V−s.

A high gain National Ignition Facility (NIF) target has a DT ice layer approximately 2.2 mm in diameter and 0.1 mm thick. This surrounds a gas volume of $V_g=4.2\times10^{-9}$ m^3 with an inner ice surface area of $S=1.3\times10^{-5}$ m^2. The power coupled into this gas volume by an electric field is

$$P_{rf}=en_e\mu_eV_gE^2, \tag{1}$$

where E is the root mean squared electric field and e is the electron charge. To reach a heat flux equivalent to the bulk heat produced by DT requires $P_{rf}=Shq_s=63$ μW. The corresponding field is $E=6.85\times10^2$ V/cm. Given the electron mobility above and the interior diameter of 2 mm, the electron transit time through the DT gas space is about 0.3 μsec. In order to avoid the loss of electron mobility as they drift into the DT ice, we choose to work at a frequency much higher than 1/(0.3 μsec). The desired field can be generated using a resonant cavity with reasonable rf power. For practical reasons we choose to apply the field at about 1 GHz. The experimental design described below allows us to generate these fields in a cryogenic microwave cavity surrounding a cell containing condensed DT.

III. EXPERIMENTAL SETUP

The cryogenic system for this experiment is designed to refrigerate a microwave cavity with variable heat loading due to varying rf power input while maintaining a cell containing DT at a constant temperature below the triple point (19.8 K). Because the rf power can be on the order of a watt, we choose to use an independent close cycle refrigerator to remove the rf power while maintaining the DT cell at constant temperature using a LHe cryostat.

A schematic of the cryogenic cooling system is shown in Fig. 1. The sample cell assembly is mounted on a controlled temperature surface which is linked to the bottom of a LHe cryostat with a variable pressure gas filled cell. This allows the sample temperature to be held just below the triple point of DT with relatively low control power. The cavity structure is hermetically sealed and attached to the control surface as well, but a thin stainless steel tube is used to thermally insulate the cavity from this surface. This design gives us a high degree of thermal decoupling between the cavity and the sample cell. Flexible thermal links are used to conduct the heat generated by the rf power to a CTI 1020 mechanical refrigerator. Our flexible coupling is an oxygen-free high-conductivity copper (OFHC) wire bundle made of strands of 0.003 in. thick OFHC copper wire wound to a diameter of about 0.5 in. Four bundles each about 1.5 in. long conduct heat out of the cavity. The sealed cavity structure serves as a secondary container for the DT in the sample cell.

Figures 2(a) and 2(b) show the sample cell region. Figure 2(a) is a cross section of the cell where the shaded part shows the region where solid DT forms. Figure 2(b) shows a quarter of the cell cut by two vertical orthogonal planes. The shaded portions of the figure show the surfaces which are

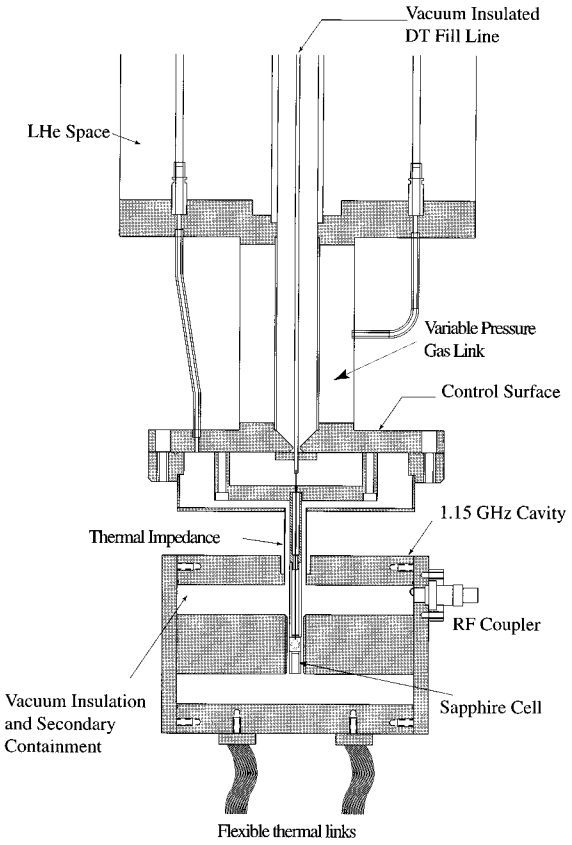

FIG. 1. Schematic diagram of lower end of cryogenic insert. The DT sample is contained within the sapphire cell. The cell is cooled by the LHe dewar. The 1.15 GHz microwave cavity is cooled by a mechanical refrigerator via flexible copper braids.

wetted by the solid DT. The parts of the sample cell inside of the rf field are made entirely from sapphire. A 5 mm diameter sapphire rod has a 3 mm hole bored through the center perpendicular to the rod axis. Flats are ground on either side of the 3 mm hole to provide a flat surface to which sapphire windows are epoxied. A sapphire ring 3 mm in diameter and 1 mm wide with a 2 mm inner diameter is positioned in the center of the 3 mm bore and epoxied in place. The inner edges of this ring are beveled to provide a 500 μm wide flat surface on the inside of the ring. A 100 μm hole in the top of the cell provides an inlet for the DT gas. The function of the ring is to provide a surface on which to image the DT ice that is not vignetted by the outside edge of the 3 mm bore. The assembled sapphire cell is epoxied to a sapphire tube which holds it in the center of the microwave cavity. This structure is attached to the control surface through a copper structure that provides tight thermal coupling.

As discussed above, this experiment requires electric fields of about 600 V/cm at a frequency large compared to 1/(0.3 μsec). A microwave cavity of a reentrant design is used as the resonant structure. This type of cavity is commonly used in klystrons and other applications where uniform microwave electric fields are desired [11]. The cavity design has a good Q factor, which produces a larger field intensity for a given power input. The field is intense and uniform between the two pole pieces where the sample is located. A cross section of this cavity is shown in Fig. 1. The cavity parts are machined from OFHC copper. The two end

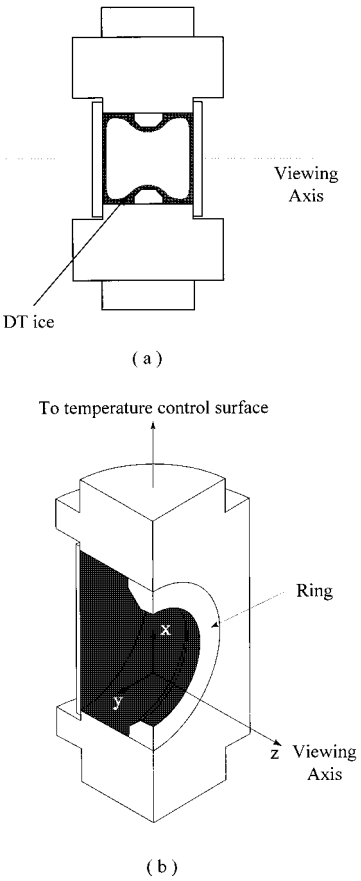

FIG. 2. Sapphire sample cell. (a) Distribution of a typical ice layer in cell after layering is complete. (b) Quarter section view of sample cell.

pieces are attached with bolts and sealed with indium gaskets to provide a vacuum tight cavity. The length is 9.14 cm and the inner diameter is 5.08 cm. The two inner poles are 4.22 cm in length and 1.27 cm in diameter. This gives a gap of 0.7 cm between the poles. Not shown are two optical windows that allow one to view the sample. They are constructed of fused silica and are 1.9 cm in diameter by 0.64 cm thick. Their clear aperture is 1.27 cm. These windows are also sealed with indium gaskets.

A wire loop coupler is used to make the transition from a coaxial waveguide to the microwave cavity. It is formed from the center conductor of the semirigid coaxial cable that carries the signal into the cavity. The size of the loop is determined empirically and adjusted to bring the VSWR (voltage standing wave ratio) of the cavity circuit as close to one as possible. Determining the size of the coupler is complicated somewhat by the temperature dependence of the resistivity of the cavity walls. A critically coupled circuit at room temperature will be over coupled at 20 K where the cavity operates. This problem is solved by first sizing the coupling loop for a room temperature cavity. The assembly is then cooled to liquid nitrogen temperature and the VSWR remeasured. The size of the loop is then adjusted to minimize the VSWR at 77 K. Final VSWR's are typically 1.16, giving a reflected power of only 0.5% of the power transmitted to the cavity. The final coupling loop is approximately rectangular, with a length of 0.75 cm and a width of 0.5 cm. The wire is 0.09 cm in diameter.

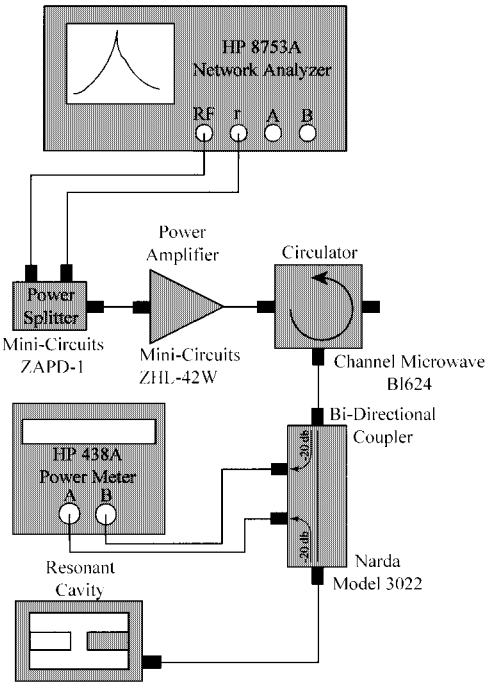

FIG. 3. Schematic layout of microwave electronics. The HP8753A Network Analyzer serves as a synthesized signal source.

Figure 3 is a diagram of the basic layout of the microwave system electronics. Our frequency source is an HP8753A network analyzer with a frequency range of 300 KHz to 3 GHz. It is needed primarily for tuning to cavity resonance and adjusting coupling when setting up the electronics system. However, its internal synthesized signal generator serves well as an accurate and stable frequency source. The power amplifier indicated in the figure has an output up to 1 W. The output power is adjusted by changing the source power from the HP8753A. The power meter is an HP438A with two 8481A sensor heads. The power meter measures incident and reflected power from the cavity via the Narda Model 3022 bi-directional coupler. The directional coupler diverts less than 1% of the signal traveling in the forward and reverse directions to the *A* and *B* inputs of the network analyzer. By measuring the ratio of transmitted and reflected power, we monitor the coupling to the cavity.

One of the more important physical quantities in this experiment is the electrical field strength in the sample cell. We have modeled the reentrant cavity design using the two-dimensional (2D) code Superfish. Using the measured loaded Q of our microwave cavity of 4070 at a VSWR of 1.16 at 19.6 K, we find that the field generated by the cavity is given by

$$E_{\mathrm{cav}} = 1950 \pm 200 \ \ \mathrm{V/cm}\sqrt{P_{rf}\ /\mathrm{W}}, \tag{2}$$

where the uncertainty is due to differences between code results and calibration measurements of the electric field [12]. This corresponds to a required rf power of 0.264 W to generate 1000 V/cm in the region between the poles with no sample cell in the gap.

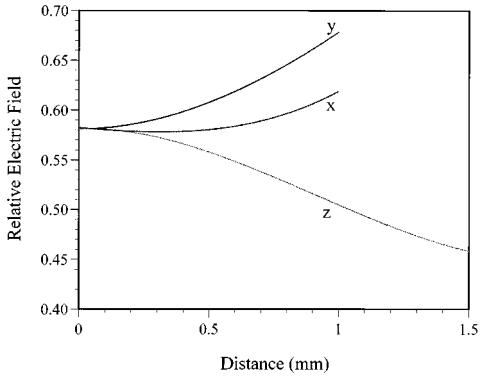

FIG. 4. Relative electrical field inside of a sample cell with a dielectric constant of 10 as compared to exterior applied field. The axis directions are indicated in Fig. 2(b).

Account must be taken of the attenuation and distortion of the electric field by the sapphire sample cell. Since the power generated in the DT gas varies as the square of the electric field, variation of the electric field distorts the isotherms in the cell and will affect the shape of the ice layer. This issue has been studied by use of finite-element analysis [13]. The static solution is suitable for determining the field of the first resonant mode of the cell, so we model the two poles as a parallel plate capacitor and hold them at opposite fixed potentials. Sapphire's dielectric constant is anisotropic and varies from 9.3 to 11.5. Since the crystalline orientation of the various components of our cell lie along different orientations, we have calculated the field inside the cell for various values of the dielectric constant in the range of sapphire and use the range of the results to estimate the uncertainty in the field inside the cell given below. The volume inside the cavity and inside the test cell are assigned a dielectric constant of one.

The magnitude of the electric field in the cell along various directions is shown in Fig. 4 for a dielectric constant of 10. The curve labeled z shows the magnitude along the axis of the hole through the sapphire, from the symmetry plane to the window. The other curves are values taken on perpendicular line segments across the circular cross section of the cell. The field strength varies from 45% to 68% of the applied field. The average magnitude of the field inside of the cell is 53% of what would be applied if no cell were in place. Using this we can write for the field inside the cell

$$E_{\text{cell}} = 950 \pm 120 \ \ \text{V/cm}\sqrt{P_{rf}\ /\text{W}}. \tag{3}$$

Therefore, to generate an average field of 1000 V/cm inside of the sample cell takes 1030 mW of rf power.

IV. DT FILL SYSTEM

In order to supply DT gas to this experiment it was necessary to develop a DT source. Palladium hydride is used extensively to store and pump hydrogen isotopes [14–16]. To carry out these experiments we have constructed a 4 gm Pd bed which is loaded with 300 Ci of DT gas. A simplified schematic is shown in Fig. 5. The hydriding reaction is reversible and is controlled by adjusting the temperature of the bed. When heated to 100 °C, hydrogen gas is released from the Pd. When cooled to LN_2 temperatures, the Pd acts as an excellent adsorber of hydrogen. Liquid helium cooled charcoal is used to pump ^{3}He generated by β decay of tritium and other potentially tritium contaminated gases in the system.

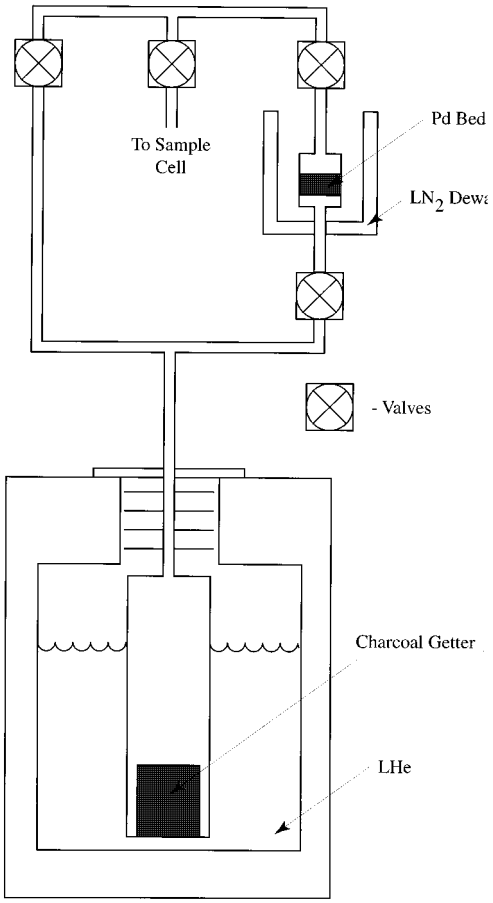

FIG. 5. Schematic of the palladium hydride source used to supply DT gas for this experiment.

V. DATA COLLECTION

The roughness of the DT ice surface is characterized optically. A long range microscope looks through windows in the cryostat and the cavity and is focused on the ring centered in the sapphire cell. Images are taken with a Photometrics camera using a Kodak KAF-1400 charge coupled device (CCD) array, and downloaded to a personal computer for analysis. Images are saved using a 1024×1024 subarray of pixels on the CCD. Each 6 μm pixel at the CCD corresponds with 2.15 μm at the focal plane. Raw images such as that shown in Fig. 6 have a bright central region which makes a transition to a dark outer region where the ice surface blocks the light. Analysis of the images consists of locating the center of the transition from light to dark as a function of angle. This is done by initially guessing the coordinates of the center of the bright region and sampling the image along radial lines emanating from the center estimate. Image intensity along the radial line is estimated at one pixel increments using a bilinear interpolation scheme. The resulting linear array of intensities is scanned to find the point of maximum derivative in intensity as an initial estimate of the location of

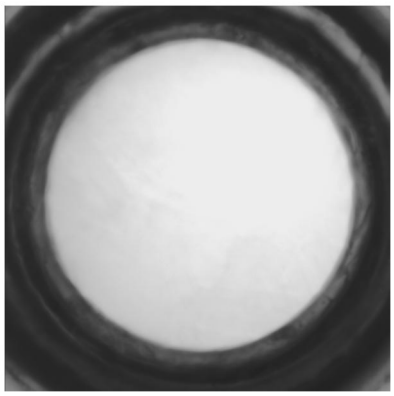

FIG. 6. DT ice layer before heating of the DT gas inside the cell.

the edge. The linear data is then fit to an error function using a Levenberg-Marquardt method allowing the center, height, baseline, and width of the fit function to vary. The center of the resulting fit function is taken as the edge location. This procedure is repeated as a function of angle to produce an array of edge radii versus angle. The center is recalculated and the entire procedure is repeated until the center estimates converge. At this point the roughness of the surface is computed by calculating the root mean square fluctuation of the edge estimates from their average, and a power spectrum of the surface fluctuations can be calculated.

VI. THERMAL ANALYSIS

In order to calculate the effect of the rf power dissipation in the DT gas on the rate at which the DT forms a uniform layer, we consider the one-dimensional case show in Fig. 7. To simplify the equations we define

$$h_1-h_2=2\Delta h,\quad h_1+h_2=h_s,\quad h_s/2=h_s',\ \text{and}\ h_g/2=h_g'. \tag{4}$$

In the three regions the general solutions for the temperatures are

$$T_a(x)=\frac{-q_s x^2}{2k_s}+C_a x\quad \text{for}\ 0\leqslant x\leqslant h_s'+\Delta h, \tag{5}$$

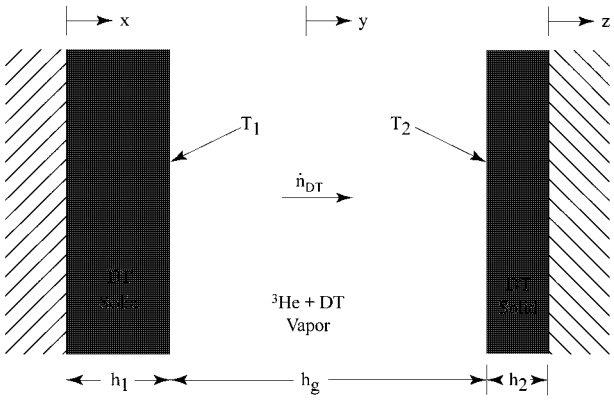

FIG. 7. Geometry and variables used in the analysis of the layering rate.

$$T_c(z)=\frac{-q_s z^2}{2k_s}+C_c z\quad \text{for}\ \Delta h-h_s'\leqslant z\leqslant 0, \tag{6}$$

$$T_b(y)=\frac{-q_g y^2}{2k_g}+C_b y+C_0\quad \text{for}\ \Delta h-h_g'\leqslant y\leqslant \Delta h+h_g', \tag{7}$$

where we have assumed $T_a(0)=T_c(0)=0$. Two conditions on the four unknowns come from the requirement of continuity of the temperatures at $x=h_s'+\Delta h$ and $y=\Delta h-h_g'$, and at $y=\Delta h+h_g'$ and $z=\Delta h-h_s'$. Two additional conditions are generated by the requirement of continuity of the heat flux at the two ice surfaces requires. These have the form

$$-k_s\left.\frac{dT_a(x)}{dx}\right|_{x=h_s'+\Delta h}=\dot{n}_{\mathrm{DT}}s-k_g\left.\frac{dT_b(y)}{dy}\right|_{y=\Delta h-h_g'}, \tag{8}$$

where $\dot{n}_{\mathrm{DT}}$ is the molecular flux of DT in the vapor space and s is heat of sublimation of DT. Using the general solutions for the temperatures these two conditions can be reduced to

$$k_s(C_a-C_c)=q_s h_s+q_g h_g\equiv Q_T, \tag{9}$$

which confirms that the total heat flux out of the system is equal to the total heat generated in the system, and

$$2q_s\Delta h-k_s(C_a+C_c)=2\dot{n}_{\mathrm{DT}}s+2q_g\Delta h-2k_g C_b. \tag{10}$$

Using the temperature continuity conditions we can solve for the temperature difference between the two ice surfaces giving

$$T_1-T_2=\frac{-\Delta h h_s q_s}{k_s}+h_s'(C_a+C_c)+\Delta h(C_a-C_c), \tag{11}$$

and

$$T_1-T_2=\frac{\Delta h h_g q_g}{k_g}-h_g C_b. \tag{12}$$

We can now use Eq. (9) to eliminate the C_a-C_c term in Eq. (11) and Eq. (10) to eliminate the C_a+C_c term, and Eq. (12) to eliminate C_b in Eq. (11) giving the result

$$(T_1-T_2)\left(1+\frac{k_g h_s}{k_s h_g}\right)=\frac{h_s}{k_s}\left\{\frac{\Delta h}{h_s}q_g h_g+q_s\Delta h-\dot{n}_{\mathrm{DT}}s\right\}. \tag{13}$$

The factor of $k_g h_s/k_s h_g$ is very small since $k_g/k_s\cong 0.04$ and $h_s/h_g\cong 0.1$, so we ignore it in the following. Using a binary diffusion model it can be shown [17] that

$$\dot{n}_{\mathrm{DT}}=\frac{Dn}{h_g n_3}\left.\frac{dn_{sv}(T)}{dT}\right|_{T=T_1}(T_1-T_2)\equiv B(T_1-T_2), \tag{14}$$

where D is the diffusion constant of the DT through the mixture of DT and ^{3}He, n is the total gas density, n_3 is the ^{3}He density, and $n_{sv}(T)$ is the density of the saturated DT vapor over the solid. Using Eq. (14) to replace T_1-T_2 in Eq. (13), and solving for $\dot{n}_{\mathrm{DT}}$ we have

$$\dot{n}_{\mathrm{DT}}=\frac{Q_T\Delta h}{\left(\frac{k_s}{B}+sh_s\right)}. \tag{15}$$

Since $\dot{n}_{\mathrm{DT}}$ is just the rate at which molecules are leaving the surface at h_1, we have

$$-\rho_s\frac{dh_1}{dt}=\rho_s\frac{dh_2}{dt}=\dot{n}_{\mathrm{DT}}, \tag{16}$$

so

$$\frac{d\Delta h}{dt}=-\frac{Q_T\Delta h/\rho_s}{\left(\frac{k_s}{B}+sh_s\right)}. \tag{17}$$

This can be integrated to give

$$\Delta h=h_0\ \exp\left[\left(-\frac{Q_T/\rho_s}{\left(\frac{k_s}{B}+sh_s\right)}\right)t\right]. \tag{18}$$

Hence, we have for the layering rate R,

$$R=\frac{Q_T/\rho_s}{\left(\frac{k_s}{B}+sh_s\right)}, \tag{19}$$

or,

$$R=\left(\frac{q_s}{s\rho_s}+\frac{q_gh_g}{sh_s\rho_s}\right)\left\{\frac{h_gk_s}{sh_sDn}\left(\left.\frac{dn_{sv}(T)}{dT}\right|_{T=T_1}\right)^{-1}n_3+1\right\}^{-1}. \tag{20}$$

The first term in parenthesis is the result of Ref. [5], and this term plus the term in braces is the result of Ref. [17]. The second term describes the effect of the heating of the gas on the layering rate. For a fixed ^{3}He concentration we expect the layering rate to increase linearly with the power dissipated in the gas, which is proportional to the power dissipated in the cavity. Since the average heat flux generated at the DT ice surface f_s is $q_gh_g/2$ in the planar case, the rate induced by the rf heating can be expressed as

$$R_{\mathrm{rf}}=\frac{f_s}{sh_s'\rho_s}\left\{\frac{h_gk_s}{sh_sDn}\left(\left.\frac{dn_{sv}}{dT}\right|_{T_1}\right)^{-1}n_3+1\right\}^{-1}. \tag{21}$$

Since this expression is independent of geometry except for the effects of ^{3}He in the braces, it should remain valid in our roughly cylindrical geometry. Since heat flux through the surface is proportional to the square of the electric field, which is proportional to the power into the cavity, we find that the layering rate is proportional to the power into the cavity for a fixed temperature and ^{3}He concentration.

VII. EXPERIMENTAL RESULTS

In order to evaluate the coupling of the electric field to the gas we first measure the rate at which freshly frozen liquid in the cell forms a uniform layer as a function of rf power into the cavity. At each rf power value we allow the ice to evolve into a uniform layer, photographing the layer in the cell at a constant rate. Each photo is analyzed as described in Sec. V and the Fourier transform of the surface fluctuations is computed. The decay of the second mode in the Fourier transform is plotted for each power and fit to an exponential. This mode has the largest initial amplitude since it is primarily caused by the vertical asymmetry in the ice layer when it freezes. The layering rate at that power is then taken as the fit coefficient of the exponential.

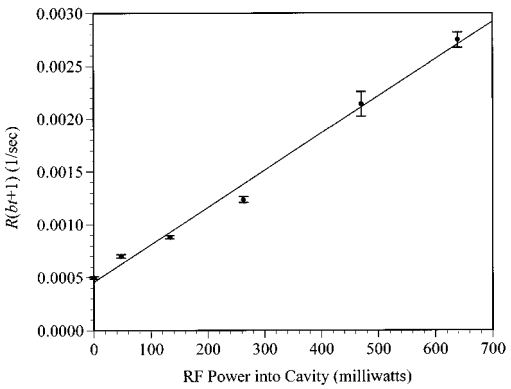

FIG. 8. Layering rates corrected for DT age vs RF power applied to the cavity.

In order to calculate the heat flux generated by the electric field we first need to evaluate the effect of the factor in braces in Eq. (21), which depends on the ^{3}He content of the vapor. To do this we fit the observed layering rates to a model of the form

$$R(P_{\mathrm{rf}},t)=\frac{aP_{\mathrm{rf}}+c}{bt+1}, \tag{22}$$

where P_{rf} is the rf power into the cavity, t is the age of the DT computed from the elapse time from the fill of the cell, and a, b, and c are fit parameters. We multiply the rates by $bt+1$ and plot the result in Fig. 8. As expected, these age corrected rates are proportional to the power into the cavity. We find $c=(4.5\pm0.7)\times10^{-4}$ sec^{-1} and $a=(3.5\pm0.3)\times10^{-3}$ sec^{-1}/W. The reciprocal of c is just the time required to form a beta layer with no ^{3}He and no rf power. Our value of c gives 36 ± 6 min which is consistent with existing data for DT [5,17]. The slope a can be used to calculate the heat flux produced and therefore the electrical conductivity of the gas. We have $aP_{\mathrm{rf}}=f_s/sh_s'\rho_s$ or

$$f_s=ash_s'\rho_sP_{\mathrm{rf}}=(2.65\pm0.27)\times10^{-3}\ \ \mathrm{W/cm^2}(P_{\mathrm{rf}}/\mathrm{W}). \tag{23}$$

Using Eq. (1) and Eq. (3)

$$\sigma_g\equiv en_e\mu_e=\frac{ash_s'\rho_s}{(V_g/S)}\,(950\ \ \mathrm{V/cm})^{-2}\ \ \mathrm{W}. \tag{24}$$

The volume to surface ratio for our cell is $(V_g/S)=3.7\times10^{-2}$ cm, however, from Fig. 4 we know that the heat production within the cell is anisotropic and consequently the heat flux at the DT ice surface is also anisotropic. This leads to uncertainty in (V_g/S), since more or less heat

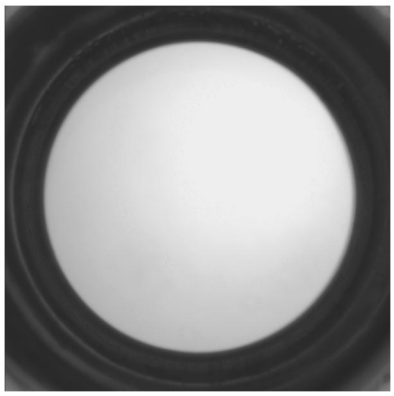

FIG. 9. DT ice layer after RF heating of the DT gas in the cell.

may flow through the surface of interest than the average over the cell. If the ring were part of a spherical surface we would have $(V_g/S)=3.3\times10^{-2}$ cm, and if it were part of a cylinder of length 2 mm, we would have $(V_g/S)=5.0\times10^{-2}$ cm. Averaging these possibilities we have $(V_g/S)=(4.0\pm0.9)\times10^{-2}$ cm. The layer thickness $h_s'=(94.4\pm5.1)$ μm. Using these we find

$$\sigma_g=(7.3\pm2.8)\times10^{-6}(\Omega-m)^{-1}. \tag{25}$$

This is consistent with the numbers quoted above for the electron density and mobility in the gas.

When rf power is applied to the cavity, there is a rapid apparent smoothing of the ice surface as seen by comparing Fig. 9 with Fig. 6. The photograph of Fig. 9 was taken after applying 315 mW of rf power to the cavity for 500 sec. This reduction is also made apparent in Fig. 10 by comparing the power spectra of the surfaces before and after applying the rf. The heat flux treated surface is smoother at all wavelengths, but the magnitude of the improvement increases at higher frequencies. Above mode 50 the rf heated surface reaches the noise level of the detection system. The lower smoothing rate at low frequencies is expected since the electric fields shown in Fig. 4 have a substantial nonuniform component. This anisotropy also complicates the analysis of the rate of improvement of the surface with rf power. As the rf field is increased, the field anisotropy induces low frequency perturbations in the ice surface even as the higher frequencies are smoothed.

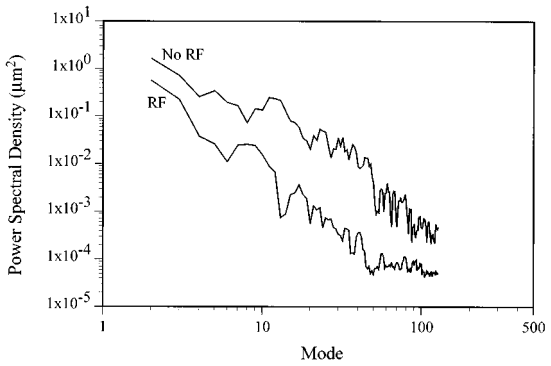

FIG. 10. Comparison of the power spectra of the DT ice surface before and after heating.

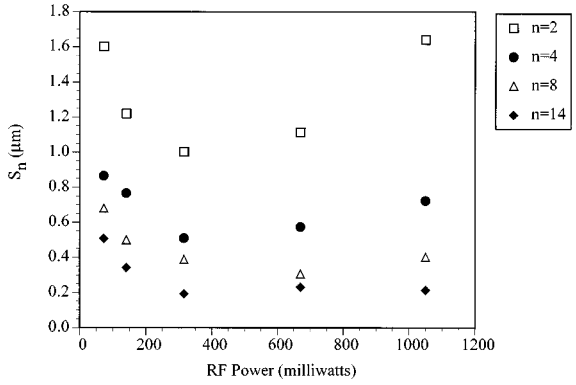

FIG. 11. S_n vs RF power for several n.

We define S_n as the rms roughness of the surface due to modes n and higher, so that

$$S_n=\left(\sum_{k=n}^{k=128} P_k\right)^{1/2}, \tag{26}$$

where P_n is the power in mode n. Figure 11 shows S_n as a function of rf power for several low values of n. As the rf power is increased, S_n initially falls but then increases as low frequency surface perturbations grow. The rate of increase falls with increasing n since the power spectrum of the electric field near the DT surface also falls rapidly with increasing n. For each n, S_n can be fit to a trial function of the form

$$S_n=a_nP_{\rm rf}+b_n/P_{\rm rf}, \tag{27}$$

where the first term represents the roughness introduced by the field anisotropy and the second represents the smoothing by the heat flux. The a_n's decrease approximately as $1/n$ and the b_n's scale approximately as $(0.13\ \mu\text{m-W})n^{-1/2}/P_{\rm rf}$. If we imagine an experiment in which a perfectly uniform field is applied we would consider only the effect of the b_n's. Then since the length of the DT surface, $L=2\pi(1\text{ mm})/n$, we can express the expected rms roughness of the heated surface using Eq. (23) as

$$S\approx\frac{0.14\ \mu\text{m}}{(f_s/\text{mW/cm}^2)}\sqrt{L/\text{mm}}. \tag{28}$$

VIII. CONCLUSIONS

We have experimentally demonstrated that a microwave frequency electric field may be used to heat DT gas inside an enclosure of solid DT. We have measured an increase in the rate at which the surface comes to equilibrium resulting from this heating. The layering rate increase has been modeled, and comparison of our data with the model gives a value for the electrical conductivity of DT gas which is in reasonable agreement with previously published results if the effect of the radiation load of the solid on the gas is considered. The enhanced thermal gradient across the gas solid interface produces a smoother solid surface than has been previously observed on beta layered surfaces. We empirically predict the surface smoothness obtainable under conditions of a perfectly uniform electric field as a function of applied power.

ACKNOWLEDGMENTS

The authors wish to thank Carlos Avalle for his assistance in making the electrical field measurements, John Burmann for his careful assembly of the sapphire sample cells, and Sam Letzring for his suggestion of the cavity design and his generous loan of microwave equipment. This work was performed under the auspices of the U.S. DOE by Lawrence Livermore National Laboratory under Contract No. W-7405-Eng-48 and by W. J. Schafer Assoc. under Contract No. DE-AC03-95SF20732.

[1] John Lindle, Phys. Plasmas **2** (11), 3393 (1995).

[2] K. Kim, L. C. Mok, M. J. Erlenborn, and T. P. Bernat, J. Vac. Sci. Technol. A **1**, 1196 (1985).

[3] J. R. Miler, Los Alamos Scientific Laboratory Report LA-6245-PR, Dec. 1975 (unpublished), p. 82; *Methods and Apparatus for Producing Cryogenic Inertially Driven Fusion Targets*, U.S. Patent 4,292,340 (Jan. 1987).

[4] A. J. Martin, R. J. Simms, and D. L. Musinski, KMS Fusion, Inc. Report No. 1348, 1985 (unpublished); A. J. Martin, R. J. Simms, and R. B. Jacobs, J. Vac. Sci. Technol. A **6**, 1885 (1988).

[5] J. K. Hoffer and L. R. Foreman, Phys. Rev. Lett. **60**, 1310 (1988).

[6] S. Hann, S. Pollaine, and J. Lindl *et al.*, Lawrence Livermore National Laboratory, UCRL-LR-105821-95-4, 1995 (unpublished), p. 81.

[7] P. Clark Souers, E. M. Fearon, and R. T. Tsugawa, Cryogenics **21**, 667 (1981).

[8] P. Clark Souers, E. M. Fearon, and R. T. Tsugawa, J. Vac. Sci. Technol. A **3**, 29 (1985).

[9] P. Clark Souers, *Hydrogen Properties for Fusion Energy* (University of California Press, Berkeley, 1986), p. 216.

[10] A. G. Robertson, Aust. J. Phys. **24**, 445 (1971).

[11] J. F. Reintjes and G. T. Coate, *Principles of Radar* (McGraw-Hill, New York, 1952), p. 636.

[12] S. Burkhart, IEEE Trans. Microwave Theory Tech. **MTT-33** (3), 262 (1985).

[13] We used the computer code Maxwell 3-D©, Ansoft Corp., Pittsburg, Pa.

[14] F. A. Lewis, *The Palladium Hydrogen System* (Academic, London, 1967).

[15] G. G. Libowitz, *The Solid State Chemistry of Binary Metal Hydrides* (Benjamin, New York, 1968).

[16] W. M. Mueller, J. P. Blackledge, and G. G. Libowitz, *Metal Hydrides* (Academic, New York, 1968).

[17] T. P. Bernat, E. R. Mapoles, and J. J. Sanchez, Lawrence Livermore National Laboratory Inertial Confinement Fusion Quarterly Report No. 2, UCRL-LR-105821-91-2, 1991 (unpublished), pp. 57–61.